Energy Selection in Nonadiabatic Transitions.

Giovanni Granucci[a], **Giacomo Melani**[a],
Maurizio Persico[a,*], **Piet Van Leuven**[b]

[a] Università di Pisa, Dipartimento di Chimica e Chimica Industriale,
via Moruzzi 13, I-56124 Pisa, Italy
[b] Vrije Universiteit Brussel, Departement Natuurkunde,
Pleinlaan 2, B-1050 Brussel, Belgium
* maurizio.persico@unipi.it

Published in J. Phys. Chem A **122**, 678-689 (2018)
DOI: 10.1021/acs.jpca.7b10146

Abstract.
In this work we investigate whether and how a molecule undergoing a nonadiabatic transition can show different energy mean values and distributions in the two electronic states that are populated. We analyse three models, of which models I and II mimick the limiting cases of almost adiabatic and almost diabatic regimes, respectively, and are solvable by first order perturbation theory. Model III represents realistically the photodissociation of a diatomic molecule and is treated numerically. The three models provide a consistent picture of the energy selection effect. For a typical avoided crossing, the wavepacket component that undegoes the transition between the two adiabatic states has a larger mean value of energy than the other component, both for upward and for downward transitions. The analysis of model II shows that the Landau-Zener rule can be deduced in a fully quantum mechanical way. We believe that the energy selection effect can be observed experimentally in the photodissociation of diatomic molecules. The effect should be particularly relevant for wavepackets endowed with a broad energy spectrum, as the result of excitation with ultrashort light pulses.

1 Introduction

Excitation of molecules with short light pulses necessarily generates wavepackets with a broad energy distribution. The ongoing tendency to decrease the pulse duration, going from femtochemistry to attochemistry,[1,2] will make this feature even more conspicuous. There are several processes occurring in the excited states that are energy selective, in the sense that their probability depends on energy and therefore the final state shows an energy bias with respect to the initial distribution. A trivial example is the photodissociation of a polyatomic molecule yielding chemically different products.

A more intriguing case is provided by nonadiabatic transitions. When the interaction that causes the transition is of nonadiabatic type, it depends directly on the momenta of the nuclei, i.e. on their kinetic energy. So, there is a reason to believe that higher energy components of the initial wavepacket have larger transition probabilities between adiabatic states. As a result, the total (electronic + nuclear) energy of a wavepacket that has undergone a transition may be displaced towards higher values with respect to the initial one. Since of course total energy is conserved, what we expect is just that the higher energy components of the initial wavepacket populate selectively the final electronic state, while the lower energy ones tend to remain in the initial state. Relevant effects may then be observed for wavepackets endowed with a broad energy spectrum, as the result of excitation with ultrashort light pulses. Clues about energy selection effects can be found in theoretical and experimental work concerning avoided crossings[3,4] and conical intersections.[5–8] Extensive tests on models showed how the transition probability between adiabatic states depends on the vibrational energy when a wavepacket goes through a conical intersection.[6] Namely, the probability increases when more energy is put in the branching plane coordinate that corresponds to the gradient difference of the two diabatic potential energy surfaces, and decreases when energy is put in the orthogonal coordinate. As a result, the energy selection effect would depend on details of the excitation process and of the energy transfer between vibrational modes, that may end up with a statistical distribution.[9] Besides the theoretical challenge of making predictions for polyatomics, it would also be hard to measure the complete energy distribution of polyatomic, or even diatomic, fragments (i.e. all the populations of roto-vibrational states). For these reasons, we prefer to investigate the simpler case of diatomics, where experimental tests are more feasible.

A bias in favour of higher kinetic energies is embodied in the Landau-Zener rule, where the transition probability depends on the nuclear velocity.[3] However, the Landau-Zener theory does not take into account the role of the electronic energy difference between the initial and final state. It is then worth to investigate whether the selection effect is the same for downward and upward transitions and how it depends on the energy gap. This is a problematic issue in semiclassical treatments: for instance, energy conservation in surface hopping is usually imposed a posteriori after each nonadiabatic event,[10–13] which can be hardly justified on quantum mechanical grounds. The theory we present is exclusively based on quantum mechanics, but our conclusions may suggest new approaches to the energy conservation problem in semiclassical dynamics.

To analyse in the simplest conditions whether and why a nonadiabatic transition can give place to two wavepackets, in the initial and in the final electronic states, with different total energy mean values and distributions, we set up three one-dimensional models. The first two models can be solved analytically by means of certain approximations, that are valid in conditions close to the adiabatic limit for the first model and to the diabatic limit for the second one. By adiabatic limit we mean a regime in which the probability of transition between adiabatic states is very small, while in the diabatic limit the same probability is close to one. In the third model, which is only solved numerically, we can span the two limiting cases and all the intermediate regimes. The three models concur in building a consistent picture where the energy difference between the two electronic states and the change in nuclear momentum due to the transition play an essential role.

2 Models I and II: perturbative solution.

In models I and II the initial wavepacket $\chi_1(q,t)$ belongs to the electronic state 1 and a new wavepacket $\chi_2(q,t)$ is created by a radiationless transition to state 2. We assume the interaction between the two electronic states to be concentrated in a limited region of the nuclear coordinate q. The wavepackets are supposed to be outside the interaction region both at the initial and final time, which will be taken to be $t = -\infty$ and $t = +\infty$. As a consequence, the total energy at the initial and final times is a sum of the two independent wavepacket energies, without an interaction energy contribution. The transition process will take place only at intermediate

times.

The two models will feature electronic potentials that only support eigenstates belonging to the continuum spectrum. This is not, however, an essential restriction in view of the energy selection effects we want to highlight. The normalized time-dependent state of the system is

$$|\Psi(q,t)\rangle = \chi_1(q,t)\ |1\rangle + \chi_2(q,t)\ |2\rangle \tag{1}$$

where $|i\rangle$ indicates an electronic state. We shall call $U_1(q)$ and $U_2(q)$ the potential energy curves of the two electronic states:

$$U_i(q) = \left\langle i \left| \hat{\mathcal{H}}_{el} \right| i \right\rangle \tag{2}$$

where $\hat{\mathcal{H}}_{el}$ is the electronic hamiltonian. We shall expand the two wavepackets in the basis of the nuclear eigenfunctions $\varphi_{i,E,n}$, where E is the eigenenergy and n is a supplementary quantum number that is needed in case of degeneracy:

$$\chi_i(q,t) = \sum_{n=1}^{g_i} \int_{E_{i,min}}^{\infty} C_{i,n}(E,t)\ e^{-iEt/\hbar}\ \varphi_{i,E,n}(q)\ dE \tag{3}$$

We call $\hat{V}$ the interaction operator and we assume $\hat{V}$ to have only off-diagonal matrix elements $\left\langle \varphi_{i,E,n} \left| \hat{V} \right| \varphi_{j,E',n'} \right\rangle$ in the electronic quantum numbers i and j. The dynamic equations for the expansion coefficients are then

$$i\hbar \frac{dC_{i,n}(E,t)}{dt} = \sum_{n'=1}^{g_j} \int_{E_{j,min}}^{\infty} \left\langle \varphi_{i,E,n} \left| \hat{V} \right| \varphi_{j,E',n'} \right\rangle e^{i(E-E')t/\hbar}\ C_{j,n'}(E',t)\ dE' \tag{4}$$

We now expand the coefficients in perturbation orders with respect to the matrix elements of the $\hat{V}$ interaction. We have non vanishing zero order coefficients $C^{(0)}_{1,n}$ only for state 1, and first order coefficients $C^{(1)}_{2,n}$ only for state 2. The zero order coefficients are constant in time and the first order ones obey the equation

$$\frac{dC^{(1)}_{2,n}(E,t)}{dt} = -\frac{i}{\hbar} \sum_{n'=1}^{g_1} \int_{E_{1,min}}^{\infty} \left\langle \varphi_{2,E,n} \left| \hat{V} \right| \varphi_{1,E',n'} \right\rangle C^{(0)}_{1,n'}(E')\ e^{i(E-E')t/\hbar}\ dE' \tag{5}$$

By integrating over time we get

$$C^{(1)}_{2,n}(E,\infty) = \\ = -2\pi i \sum_{n'=1}^{g_1} \int_{E_{1,min}}^{\infty} \left\langle \varphi_{2,E,n} \left| \hat{V} \right| \varphi_{1,E',n'} \right\rangle C^{(0)}_{1,n'}(E')\ \delta(E-E')\ dE' \quad (6)$$

If $E < E_{1,min}$, then $C^{(1)}_{2,n}(E,\infty) = 0$, otherwise

$$C^{(1)}_{2,n}(E,\infty) = -2\pi i \sum_{n'=1}^{g_1} \left\langle \varphi_{2,E,n} \left| \hat{V} \right| \varphi_{1,E,n'} \right\rangle C^{(0)}_{1,n'}(E) \quad (7)$$

This simple first-order perturbation theory solution (FOPT) will allow us to highlight the physical origin of the energy selection effect in models I and II and to apply the same concepts in interpreting the numerical results of model III.

In both models I and II the potential of the initial state is constant, $U_1(q) = 0$. Then, the energy eigenstates are also momentum eigenstates:

$$\varphi_{1,k_1,\pm}(q) = (2\pi)^{-1/2}\ e^{\pm ik_1 q} \quad (8)$$

where $k_1 = (2mE)^{1/2}/\hbar$ and m is the reduced nuclear mass. The quantum number n can be identified with the sign of the momentum $\pm\hbar k_1$. Note that $\varphi_{1,k_1,\pm}$ is normalized to $\delta(k_1 - k_1')$, while the energy normalized eigenstate is

$$\varphi_{1,E,\pm}(q) = \frac{m^{1/2}}{(2\pi k_1)^{1/2}\hbar}\ e^{\pm ik_1 q} \quad (9)$$

The wavepacket in state 1 will be assumed to be of gaussian shape,[14] i.e. in the momentum representation:

$$\tilde{\chi}_1(\pm k_1, t) = 2^{1/4}\pi^{-1/4}\sigma_0^{1/2}\ e^{-\sigma_0^2(\pm k_1 - k_0)^2}\ e^{-i\hbar k_1^2 t/2m} \quad (10)$$

In the coordinate representation we have

$$\chi_1(q,t) = (2\pi)^{-1/4}\sigma_0^{1/2}\left(\sigma_0^2 + \frac{i\hbar t}{2m}\right)^{-1/2} exp\left[-\frac{(q-vt)^2}{4\left(\sigma_0^2 + \frac{i\hbar t}{2m}\right)} + ik_0\left(q - \frac{vt}{2}\right)\right] \quad (11)$$

Here $v = \hbar k_0/m$ and σ_0 is the minimum position uncertainty, that is reached at $t = 0$. The center of the wavepacket is $q = 0$ at $t = 0$. The coefficients of the energy eigenstates (9) are

$$C^{(0)}_{1,\pm}(E) = \frac{2^{1/4}(m\sigma_0)^{1/2}}{\pi^{1/4}\hbar k_1^{1/2}}\, e^{-\sigma_0^2(\pm k_1 - k_0)^2} \tag{12}$$

Considering that we get the same initial energy $E = \hbar^2 k_1^2/2m$ with two opposite values of the momentum, the energy distribution is

$$\rho_1(E) = \left|C^{(0)}_{1,+}(E)\right|^2 + \left|C^{(0)}_{1,-}(E)\right|^2 = \frac{2^{1/2} m\sigma_0}{\pi^{1/2}\hbar^2 k_1}\left[e^{-2\sigma_0^2(k_1-k_0)^2} + e^{-2\sigma_0^2(k_1+k_0)^2}\right] \tag{13}$$

(remember that $k_1 = \sqrt{2mE}/\hbar$). In this expression, the two gaussian terms in square brackets represent the contributions of positive momenta (the one with $k_1 - k_0$) and of negative momenta (the one with $k_1 + k_0$). If $k_0 \gg \sigma_0^{-1}$, only the former counts, the latter being much smaller.

3 Model 1: two constant potentials.

As a first example we take the extremely simple case where both the adiabatic potentials are constant: $U_1(q) = 0$ and $U_2(q) = D$. The expressions for $\varphi_{2,k_2,\pm}(q)$ and $\varphi_{2,E,\pm}(q)$ are analogous to eqs. (8) and (9), but $k_2 = \sqrt{2m(E-D)}/\hbar$.

We shall consider two alternative definitions of the interaction $\hat{V}$. The first is of electronic type, such as the spin-orbit interaction, and is represented as a simple function of q. The second is of nonadiabatic type, which means it contains derivative operators with respect to q.

3.1 Model Ia: electronic type interaction.

For the electronic type interaction we shall assume a gaussian shape:

$$\hat{V} \equiv V(q) = V_0\, e^{-q^2/4\sigma_V^2} \tag{14}$$

Then

$$\left\langle \varphi_{2,E,s_2} \left| \hat{V} \right| \varphi_{1,E,s_1} \right\rangle = \frac{m\sigma_V V_0}{\pi^{1/2}\hbar^2 (k_1 k_2)^{1/2}}\, e^{-\sigma_V^2(s_1 k_1 - s_2 k_2)^2} \tag{15}$$

Here s_1 and s_2 are the signs of the momenta in the eigenfunctions φ_{1,E,s_1} and φ_{2,E,s_2}. From eq. (7) we get

$$C^{(1)}_{2,\pm}(E,\infty) = \frac{2\pi^{1/2} i\ m\sigma_V V_0}{\hbar^2 (k_1 k_2)^{1/2}} \left[e^{-\sigma_V^2 (k_1 \mp k_2)^2}\ C^{(0)}_{1,+}(E) + e^{-\sigma_V^2 (k_1 \pm k_2)^2}\ C^{(0)}_{1,-}(E) \right] \tag{16}$$

The final energy distribution in state 2 is therefore

$$\begin{aligned} \rho_2(E) &= \left| C^{(1)}_{2,+}(E,\infty) \right|^2 + \left| C^{(1)}_{2,-}(E,\infty) \right|^2 = \\ &= \frac{4(2\pi)^{1/2} m^3 \sigma_0 (\sigma_V V_0)^2}{\hbar^6 k_1^2 k_2} \left\{ \left[e^{-\sigma_V^2 (k_1-k_2)^2 - \sigma_0^2 (k_1-k_0)^2} + e^{-\sigma_V^2 (k_1+k_2)^2 - \sigma_0^2 (k_1+k_0)^2} \right]^2 + \right. \\ &\qquad \left. + \left[e^{-\sigma_V^2 (k_1+k_2)^2 - \sigma_0^2 (k_1-k_0)^2} + e^{-\sigma_V^2 (k_1-k_2)^2 - \sigma_0^2 (k_1+k_0)^2} \right]^2 \right\} \end{aligned} \tag{17}$$

The density $\rho_2(E)$ vanishes for either $E < D$ or $E < 0$, i.e. for $E < \max(0, D)$. Note that the energy distribution does not depend on the V_0 parameter, that appears only as a multiplicative factor.

The largest exponential term in expression (17) is $exp[-\sigma_V^2 (k_1 - k_2)^2 - \sigma_0^2 (k_1 - k_0)^2]$. If we introduce the "central" kinetic energy of the initial wavepacket $E_0 = \hbar^2 k_0^2 / 2m$, all the exponents in eq. (17) contain the terms $-2m\sigma_0^2 (\sqrt{E} \pm \sqrt{E_0})^2/\hbar$ and $-2m\sigma_V^2 (\sqrt{E} \pm \sqrt{E - D})^2/\hbar$. With reasonable values of the reduced mass and of the position uncertainty (for the latter, take for instance the usual vibrational amplitudes), $2m\sigma_0^2/\hbar \approx 10^2$ a.u. or larger. If $V(q)$ does not undergo abrupt changes as a function of q, $2m\sigma_V^2/\hbar$ is likely to be even larger. So, if m, σ_0, σ_V and E_0 are not too small, we can neglect all the exponentials in eq. (17) except the first one:

$$\rho_2(E) \simeq \left| C^{(1)}_{2,+}(E,\infty) \right|^2 \simeq \frac{4(2\pi)^{1/2} m^3 \sigma_0 (\sigma_V V_0)^2}{\hbar^6 k_1^2 k_2}\ e^{-2\sigma_V^2 (k_1-k_2)^2 - 2\sigma_0^2 (k_1-k_0)^2} \tag{18}$$

In the approximation of eq. (18), the probability ratio for a given energy component of the initial wavepacket is

$$R(E) = \frac{\rho_2(E)}{\rho_1(E)} \simeq \frac{4\pi m^2 (\sigma_V V_0)^2}{\hbar^4 k_1 k_2}\ e^{-2\sigma_V^2 (k_1-k_2)^2} \tag{19}$$

The energy dependence of the ratio $R(E)$ shows that the nonadiabatic transition introduces a bias towards larger energies. Note that we are interested

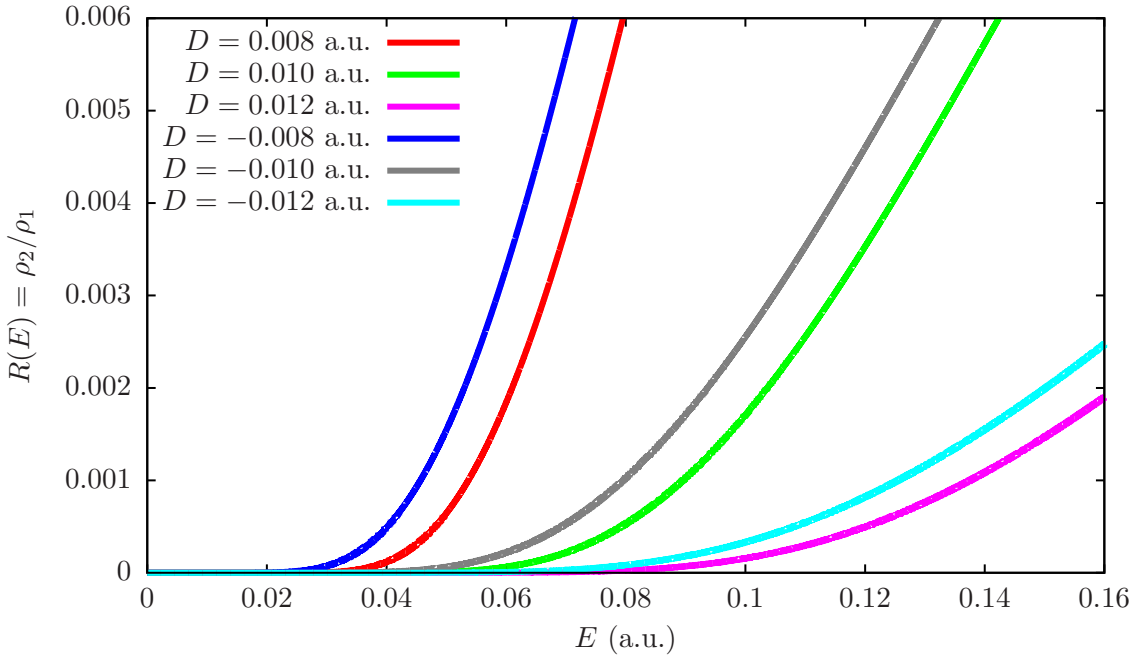

Figure 1: Probability ratio as a function of E, i.e. the ratio of the final to initial energy distributions $R(E) = \rho_2(E)/\rho_1(E)$, eq. (19). The relevant parameters are $m = 5000$ a.u., $\sigma_V^2 = 1$ a.u. and $V_0 = 0.001$ a.u. Six different values of D are tried.

in energies not too far from E_0, where the initial state probability is largest. $R(E)$ depends on energy through two factors

$$f(E) = \frac{1}{k_1 k_2} = \frac{\hbar^2}{2m\sqrt{E(E-D)}} \tag{20}$$

and the exponential

$$g(E) = e^{-2\sigma_V^2(k_1-k_2)^2} = e^{-4m\sigma_V^2(\sqrt{E}-\sqrt{E-D})^2/\hbar^2} \tag{21}$$

The former factor is required to switch from the momentum to the energy distribution. It is a decreasing function of E and diverges at the lower limit of the energy range ($E = \max(0, D)$). On the contrary, the exponential factor $g(E)$ is an increasing function of E that takes the value $exp(-4m\sigma_V^2|D|)$ at

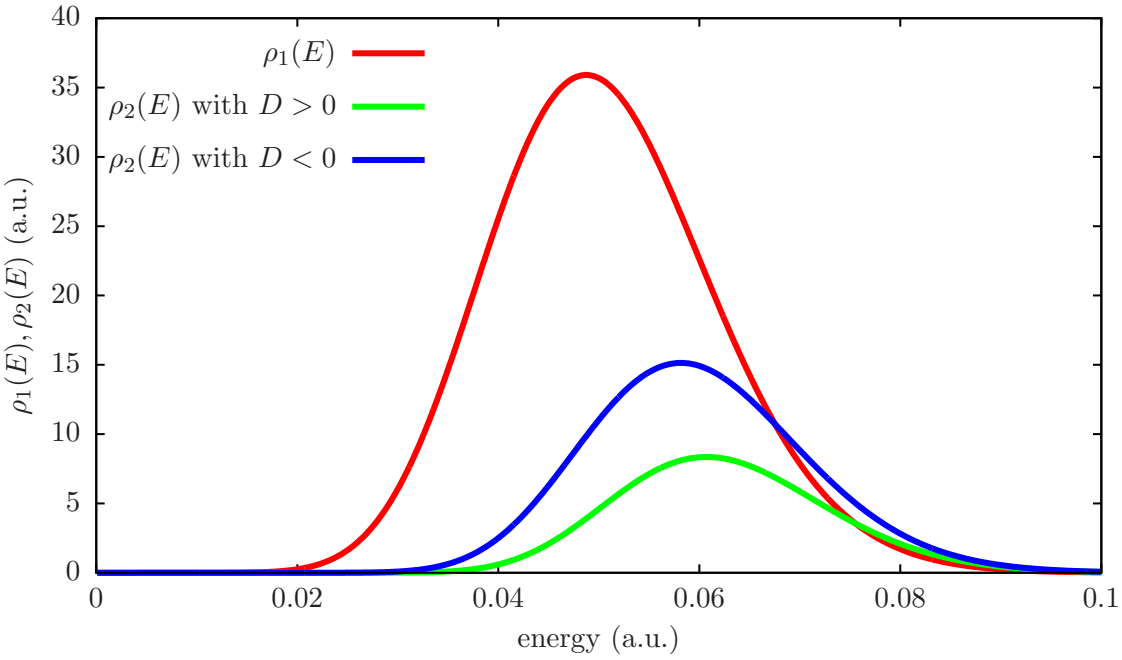

Figure 2: Initial and final energy distributions for model Ia, eqs. (13) and (17), respectively. The model parameters are: $m = 5000, D = \pm 0.008, V_0 = 0.001, \sigma_V = 1, \sigma_0 = 0.2, E_0 = 0.05$ (all in a.u.). $\rho_2(E)$ is amplified by a factor 200.

$E = \max(0, D)$. Unless D is close to zero, which would be hardly consistent with quasi-adiabatic conditions, the starting value of $g(E)$ is so small that the increase of $R(E)$ for E approaching $E = \max(0, D)$, due to the $f(E)$ factor, is confined to a very limited range of energies (not even detectable in fig. 1).

The factor $g(E)$ shows that a large change of the nuclear momentum as a result of the electronic transition is unlikely. In fact, two flat potentials have no effect on the momenta, only the weak $V(q)$ interaction has. Moreover, the momentum can change only during the limited time spent by the wavepacket in the interaction region. Since the total energy cannot change but the potential energy does, the kinetic energy must decrease or increase by D when switching from electronic state 1 to 2. The corresponding variation in

the momentum is

$$(k_2 - k_1)^2 = \frac{2m}{\hbar^2} \left[(E-D)^{1/2} - E^{1/2}\right]^2 = \frac{mD^2}{2\hbar^2 E} + O(E^{-2}) \tag{22}$$

We see that the momentum difference decreases with energy and vanishes for $E \to \infty$, so the $g(E)$ function goes to the asymptotic value of 1 at large energies. The bias towards larger energies due to the momentum/energy matching effect, for a wavepacket with an energy spectrum extending from $E + \Delta$ to $E - \Delta$, can be quantified as

$$\frac{g(E+\Delta)}{g(E-\Delta)} \simeq exp\left(\frac{2m\sigma_V^2 D^2}{\hbar^2} \frac{\Delta}{E^2 - \Delta^2}\right) \tag{23}$$

The bias will be more effective the larger the potential energy difference D and the broadness of the wavepacket Δ. On the contrary, higher central energies E will decrease the effect.

In fig. 2 we show $\rho_1(E)$ and $\rho_2(E)$ for a set of physically plausible parameters (all in a.u.): $m = 5000, D = \pm 0.008, V = 0.001, \sigma_V = 1, \sigma_0 = 0.2, E_0 = 0.05$. The total transition probability is very small, of the order of 0.1-0.2%. We see that the final energy distribution is displaced at higher energies with respect to the initial one, even with $D < 0$, because this allows to satisfy at once the rigorous energy conservation and the approximate momentum conservation, as already highlighted by eq. (22) and fig. 1. We find lower transition probabilities and slightly higher energies with $D > 0$ than with $D < 0$. In both cases the energy bias due to the electronic transition is not negligible and should be experimentally detectable in a real system with similar or equivalent molecular parameters.

In Table 1 we compare the predictions of FOPT with the results of accurate numerical calculations performed with a standard method.[15] In both cases the transition probability is computed as

$$P_{12} = \int_0^\infty \rho_2(E)\, dE \tag{24}$$

while the averaged energy difference between the final wavepackets in state 2 and state 1 is

$$\Delta\langle E\rangle = \frac{\int_0^\infty \rho_2(E)\, E\, dE}{\int_0^\infty \rho_2(E)\, dE} - \frac{\int_0^\infty \rho_1(E)\, E\, dE}{\int_0^\infty \rho_1(E)\, dE} \tag{25}$$

		P_{12}		$\Delta\langle E\rangle$	
D	V_0	FOPT	num.	FOPT	num.
0.008	0.00025	0.0000687	0.0000670	0.01202	0.01212
0.008	0.00100	0.0010999	0.0007141	0.01202	0.01379
0.008	0.00200	0.0043997	0.0006850	0.01202	0.01736
-0.008	0.00025	0.0001276	0.0001249	0.00942	0.00949
-0.008	0.00100	0.0020417	0.0014299	0.00942	0.01073
-0.008	0.00200	0.0081670	0.0016422	0.00942	0.01550

Table 1: Transition probabilities P_{12} and averaged energy differences $\Delta\langle E\rangle$ (a.u.) obtained for model Ia with different values of the interaction parameter V_0. All other parameters as in the example of Fig. 2. First-order perturbation theory (FOPT) predictions are compared with accurate numerical results.

The FOPT results are obtained with ρ_1 and ρ_2 supplied by eqs. (13) and (17). Table 1 shows that in the limit of small couplings FOPT is quite accurate, but the predicted transition probability deteriorates rapidly as V_0 increases. Even probabilities of the order of 1% are not accurately reproduced, probably because when the wavepacket goes through the interaction region the population of the initial state decreases by large amounts, orders of magnitude larger than the final result, thus contradicting the basic assumption of FOPT. However, the averaged energy differences agree reasonably with the exact ones and in particular the latter are not much affected by the value of V_0. We conclude that this level of theory is adequate for an understanding of the energy selection effects.

3.2 Model Ib: nonadiabatic type interaction.

We now replace the coupling $\hat{V}$ with two nonadiabatic operators $\hat{W}_{12}$ and $\hat{W}_{21}$:

$$\hat{W}_{ij} = -\frac{1}{m}\left[g_{ij}(q)\frac{\partial}{\partial q} + \frac{1}{2}\frac{\partial g_{ij}}{\partial q}\right] \tag{26}$$

where $g_{12} = \left\langle \psi_1 \left| \frac{\partial}{\partial q} \right| \psi_2 \right\rangle$ and ψ_i is an electronic wavefunction.[16] The coupling function g_{12} is again assumed to be a gaussian function and $g_{21} = -g_{12}$:

$$g_{12}(q) = W_0\, e^{-q^2/4\sigma_W^2} \tag{27}$$

Then eq. 15 is replaced by:

$$\left\langle \varphi_{2,E,s_2} \left| \hat{W}_{21} \right| \varphi_{1,E,s_1} \right\rangle = \frac{i\sigma_W W_0}{2\pi^{1/2}\hbar^2} \, \frac{s_1 k_1 + s_2 k_2}{(k_1 k_2)^{1/2}} \, e^{-\sigma_W^2 (s_1 k_1 - s_2 k_2)^2} \tag{28}$$

and

$$\begin{aligned} C^{(1)}_{2,\pm}(E,\infty) &= \frac{\pi^{1/2}\sigma_W W_0}{\hbar^2 (k_1 k_2)^{1/2}} \cdot \\ &\cdot \left[(k_1 \pm k_2) e^{-\sigma_W^2 (k_1 \mp k_2)^2} \, C^{(0)}_{1,+}(E) - (k_1 \mp k_2) e^{-\sigma_W^2 (k_1 \pm k_2)^2} \, C^{(0)}_{1,-}(E) \right] \end{aligned} \tag{29}$$

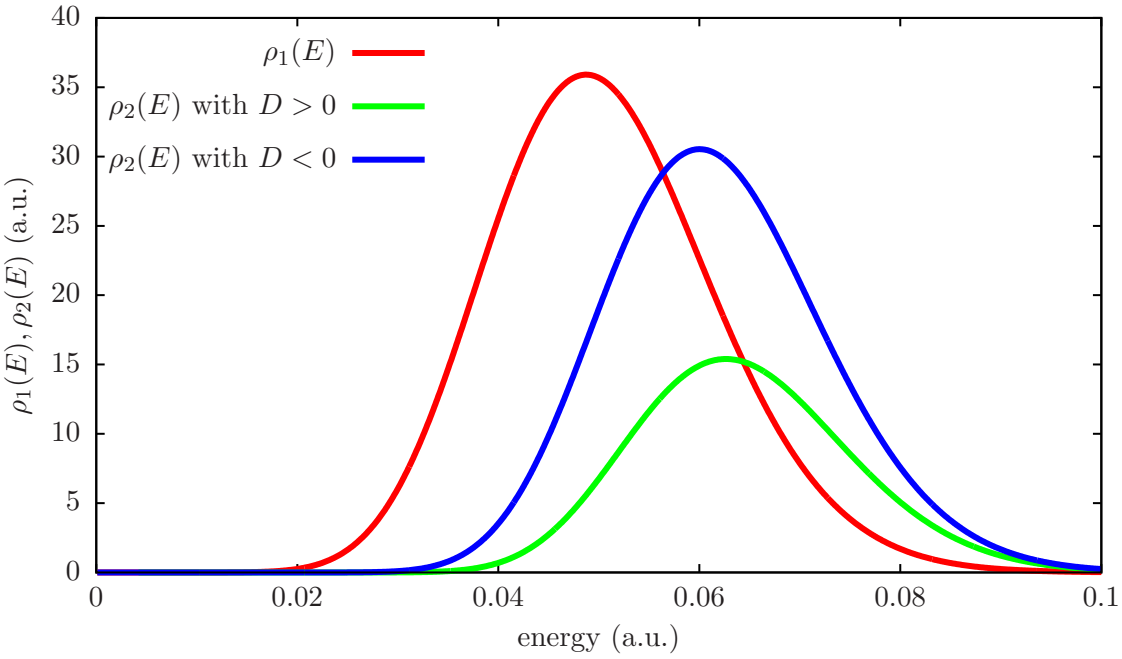

Figure 3: Initial and final energy distributions for model Ib, eqs. (13) and (30), respectively. The model parameters are: $m = 5000, D = \pm 0.008, W_0 = 0.2, \sigma_W = 1, \sigma_0 = 0.2, E_0 = 0.05$ (all in a.u.). $\rho_2(E)$ is amplified by a factor 400.

The final energy distribution in state 2 is

$$\rho_2(E) = \frac{(2\pi)^{1/2} m\sigma_0(\sigma_W W_0)^2}{\hbar^6 k_1^2 k_2} \cdot$$
$$\cdot \left\{ \left[(k_1+k_2) e^{-\sigma_W^2(k_1-k_2)^2 - \sigma_0^2(k_1-k_0)^2} - (k_1-k_2) e^{-\sigma_W^2(k_1+k_2)^2 - \sigma_0^2(k_1+k_0)^2} \right]^2 + \right.$$
$$\left. + \left[(k_1-k_2) e^{-\sigma_W^2(k_1+k_2)^2 - \sigma_0^2(k_1-k_0)^2} - (k_1+k_2) e^{-\sigma_W^2(k_1-k_2)^2 - \sigma_0^2(k_1+k_0)^2} \right]^2 \right\} \tag{30}$$

As before, $\rho_2(E) = 0$ for $E < \max(0, D)$ and, with the same considerations as in case Ia, we can approximate ρ_2 as

$$\rho_2(E) \simeq \frac{(2\pi)^{1/2} m\sigma_0(\sigma_W W_0)^2}{\hbar^6 k_1^2 k_2} (k_1+k_2)^2 \, e^{-2\sigma_W^2(k_1-k_2)^2 - 2\sigma_0^2(k_1-k_0)^2} \tag{31}$$

Also, the energy distributions of eqs. (30) or (31) are independent on the coupling parameter W_0. The main difference with respect to the purely electronic coupling case are the factors $(k_1 \pm k_2)$ that enter this formula because of the derivative operator contained in $\hat{W}_{ij}$. Physically, this means that the faster or more energetic components of the wavepacket are more likely to undergo the nonadiabatic transition, not only because of the easier

		P_{12}		$\Delta\langle E\rangle$	
D	W_0	FOPT	num.	FOPT	num.
0.008	0.05	0.0000644	0.0000630	0.01395	0.01399
0.008	0.10	0.0002577	0.0002357	0.01395	0.01411
0.008	0.20	0.0010308	0.0007124	0.01395	0.01467
0.008	0.40	0.0041233	0.0006753	0.01395	0.01828
-0.008	0.05	0.0001306	0.0001280	0.01127	0.01130
-0.008	0.10	0.0005225	0.0004812	0.01127	0.01140
-0.008	0.20	0.0020900	0.0014881	0.01127	0.01183
-0.008	0.40	0.0083602	0.0016324	0.01127	0.01464

Table 2: Transition probabilities P_{12} and averaged energy differences $\Delta\langle E\rangle$ (a.u.) obtained for model Ib with different values of the interaction parameter W_0. All other parameters as in the example of Fig. 3. First-order perturbation theory (FOPT) predictions are compared with accurate numerical results.

matching of energy and momentum, but also because of the more effective coupling. Figure 3 shows the $\rho_1(E)$ and $\rho_2(E)$ energy distributions with $\sigma_W = 1$ and $W_0 = 0.2$ a.u. All the other model parameters are the same as in Figure 2. We see that the $\rho_2(E)$ distributions are further displaced towards high energies with respect to those of model Ia, but the difference is small and with these parameters the energy/momentum matching effect is clearly more important than the increase of the coupling strength with energy.

In Table 2 we compare the predictions of FOPT with the results of accurate numerical calculations, as we did in the previous section for model Ia. The FOPT density ρ_2 is here given by eq. (30). Again, for small couplings the FOPT results are accurate while for larger couplings P_{12} is overestimated, but $\Delta\langle E\rangle$ is rather well reproduced.

4 Model II: avoided crossing.

This model is defined by two diabatic potentials that cross each other at $q = 0$. Here the coupling $\hat{V}$ is again a mere function of q, but for maximum simplicity we shall assume it constant. Because of this off-diagonal electronic matrix element the crossing is avoided in the adiabatic representation. However, we shall stick to the diabatic represention, because we want to treat the quasi-diabatic limiting case, i.e. a weakly avoided crossing. As in the Landau-Zener model, the potentials are linear functions of q. As a further simplification, the potential U_1 that hosts the initial wavepacket is constant:

$$U_1(q) = 0 \qquad U_2(q) = -F\ q \qquad V(q) = V_0 \tag{32}$$

The eigenfunctions in the diabatic state 1 are the same as in eq. (9). The eigenfunctions in the diabatic state 2 obey the Schrödinger equation

$$\left(-\frac{\hbar^2}{2m}\frac{d^2}{dq^2} - F\ q - E\right)\varphi_{2,E}(q) = 0 \tag{33}$$

By substituting

$$q = \frac{x}{\beta} + q_0 \tag{34}$$

with $\beta = -\left(2\hbar^{-2}mF\right)^{1/3}$ and $q_0 = -E/F$ we reduce to Airy's equation[18]

$$\left(\frac{d^2}{dx^2} - x\right)\ A(x) = 0 \tag{35}$$

The standard solution $A(x)$ can be expressed through its Fourier transform:

$$\tilde{A}(\omega) = (2\pi)^{-1/2} e^{i\omega^3/3} \tag{36}$$

The (unnormalized) eigenfunctions are then

$$\varphi_{2,E}(q) = A(-\beta(q - q_0)) \tag{37}$$

and their Fourier transforms

$$\tilde{\varphi}_{2,E}(\omega) = -\beta^{-1}\ \tilde{A}(-\beta^{-1}\omega)\ e^{-i\omega q_0} \tag{38}$$

Since

$$\langle \varphi_{2,E} \,|\varphi_{2,E'} \rangle = \langle \tilde{\varphi}_{2,E} \,|\tilde{\varphi}_{2,E'} \rangle = \frac{F}{\beta^2}\ \delta(E - E') \tag{39}$$

normalization requires

$$\tilde{\varphi}_{2,E}(\omega) = -(2\pi)^{-1/2} F^{-1/2}\ e^{-i(\beta^{-3}\omega^3/3 + \omega q_0)} \tag{40}$$

The interaction matrix element is

$$\left\langle \varphi_{2,E} \left| \hat{V} \right| \varphi_{1,E,\pm} \right\rangle = -\frac{m^{1/2} V_0}{(2\pi F k)^{1/2}\hbar} e^{\pm i(\beta^{-3}k^3/3 + k q_0)} \tag{41}$$

where $k = \sqrt{2mE}/\hbar$.

If we are close to the diabatic limit, we can resort to the perturbation theory developed in section 2 and obtain

$$C_2^{(1)}(E, \infty) = \frac{(2\pi)^{1/2} i\ m^{1/2} V_0}{(Fk)^{1/2}\hbar} \left[e^{i(\beta^{-3}k^3/3 + k q_0)}\ C_{1,+}^{(0)}(E) + e^{-i(\beta^{-3}k^3/3 + k q_0)}\ C_{1,-}^{(0)}(E) \right] \tag{42}$$

and

$$\begin{aligned} \rho_2(E) &= \frac{(8\pi)^{1/2}\ m^2 \sigma_0 V_0^2}{F k^2 \hbar^4} \cdot \\ &\cdot \left[e^{-2\sigma_0^2 (k - k_0)^2} + e^{-2\sigma_0^2 (k + k_0)^2} + 2\ e^{-2\sigma_0^2 (k^2 + k_0^2)}\ cos(2\beta^{-3}k^3/3 + 2k q_0) \right] \end{aligned} \tag{43}$$

By considering only the positive momentum component, the ratio $\rho_2(E)/\rho_1(E)$ can be approximated as

$$R(E) \simeq \frac{|C_2^{(1)}(E,\infty)|^2}{|C_{1,+}^{(0)}(E)|^2} = \frac{2\pi m V_0^2}{\hbar^2 F\ k} = \frac{2^{1/2}\pi m^{1/2} V_0^2}{\hbar F\ E^{1/2}} \tag{44}$$

Within this model, $R(E)$ is a diabatic transition probability, i.e. it is the probability to remain in the same adiabatic state. The probability P_{adia} to switch to the other adiabatic state is $1 - R(E)$. Since $\hbar k/m$ is the speed v at which the wave $\varphi_{1,E,+}$ travels, our estimate of P_{adia} is approximately equal to the Landau-Zener one:

$$P_{LZ} = e^{-2\pi V_0^2/(\hbar v F)} \simeq 1 - R(E) \tag{45}$$

This equality is valid to first order in $R(E)$. Since the Landau-Zener rule is valid in the semiclassical framework under certain conditions that are met only near the diabatic limit, we do not need a more accurate identity than eq. (45) to state that the Landau-Zener rule holds also in a fully quantum mechanical treatment.

The diabatic transition probability $R(E)$ is a simple decreasing function of E, so we expect a behaviour qualitatively similar to that of model I: the wavepacket that remains on the same adiabatic state (here, the smaller component χ_2) has a lower energy than the one that makes the nonadiabatic transition (here, the larger component χ_1). The energy selection effect is here due to the coupling matrix element, as in the nonadiabatic model Ib, and more precisely to the $k = \sqrt{2mE}/\hbar$ factor in the denominator of $\left|\left\langle \varphi_{2,E} \middle| \hat{V} \middle| \varphi_{1,E,\pm} \right\rangle\right|^2$. At variance with models Ia and Ib, here we see no influence of the energy/momentum matching, because the transition takes place when the electronic states are almost degenerate. In fact the V_0 parameter only enters the $\rho_2(E)$ function as a multiplicative factor (see eq. (43)), so it does not affect the shape of the distribution and the energy selection. Moreover, if $\sigma_0 k_0 \gg 1$, as already noted the energy distributions in state 1 and 2 are approximately proportional to two simple functions of E:

$$\rho_1(E) \propto \frac{1}{k_1} e^{-2\sigma_0^2(k_1-k_0)^2} \tag{46}$$

and

$$\rho_2(E) \propto \frac{1}{k_1^2} e^{-2\sigma_0^2(k_1-k_0)^2} \tag{47}$$

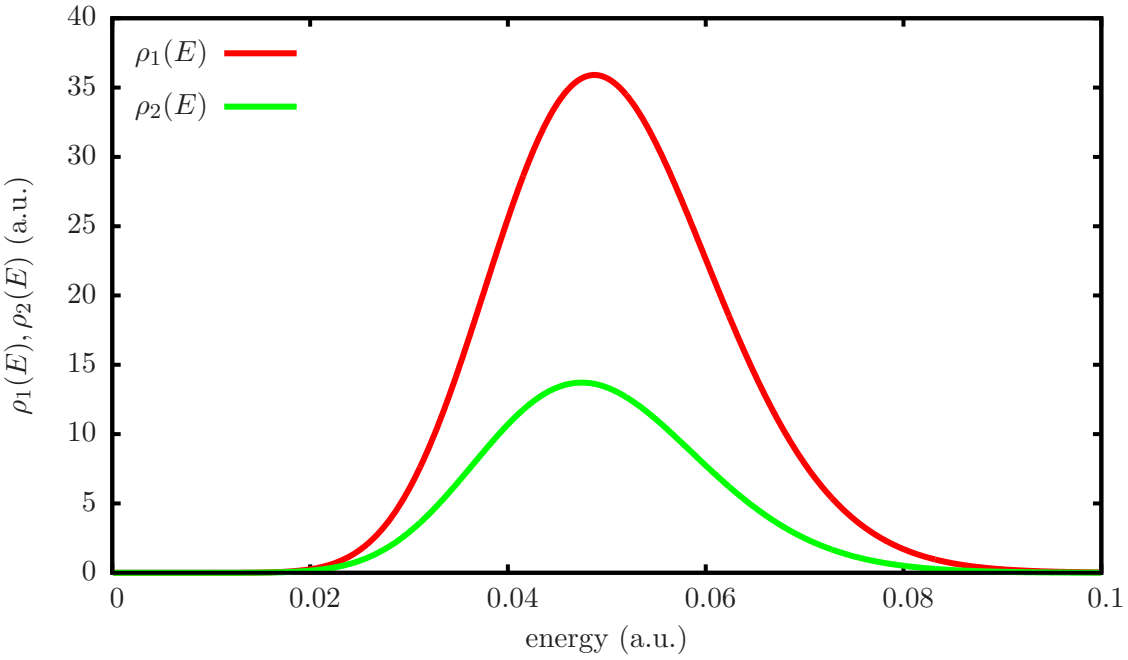

Figure 4: Initial and final energy distributions for the avoided crossing model II, eqs. (13) and (43), respectively. The relevant parameters are: $m = 5000, F = 0.03, V_0 = 0.002, E_0 = 0.05, \sigma_0 = 0.2$, all in atomic units. ρ_2 is multiplied by 2.

Computing average energy differences $\Delta\langle E\rangle$ between the two states implies elliptic integrals, but we can approximate $\Delta\langle E\rangle$ with the displacement of the maxima of the two distributions. By requiring $d\rho_1(E)/dE = 0$ we get

$$k_1 = \frac{k_0}{2}\left(1 \pm \sqrt{1 - \sigma_0^{-2}k_0^{-2}}\right) \tag{48}$$

We choose the solution closer to k_0 and we approximate the square root in the assumption that $\sigma_0^{-2}k_0^{-2} \ll 1$. Then

$$k_1 \simeq k_0 - \frac{1}{4\sigma_0^2 k_0} \tag{49}$$

This amounts to say that the maximum of $\rho_1(E)$ is found at

$$E_1 \simeq E_0 - \frac{\hbar^2}{4m\sigma_0^2} \tag{50}$$

In a similar way, for $\rho_2(E)$ one finds

$$E_2 \simeq E_0 - \frac{\hbar^2}{2m\sigma_0^2} \tag{51}$$

So, the displacement of the maxima is

$$\Delta E_{max} = E_2 - E_1 \simeq -\frac{\hbar^2}{4m\sigma_0^2} \tag{52}$$

We see that, provided the momentum uncertainty $\Delta k = 1/2\sigma_0$ is well below the central value k_0, the energy selection effect is also independent on k_0 or E_0 and is proportional to Δk^2.

In Figure 4 we show the distributions for this model, with the same parameters as in Figures 2 and 3, where applicable. We see that lower energies are favoured in the transition, but the difference between ρ_1 and ρ_2 is much smaller than in model I. This was expected, since the momentum/energy matching effect is absent in this case. The average energy difference, obtained by numerical integration, is very close to $-(4m\sigma_0^2)^{-1} = -0.00127$ a.u.

In Table 3 we compare the predictions of FOPT with the results of accurate numerical calculations, as we did in the previous sections for models Ia and Ib. The FOPT density ρ_2 is here given by eq. (43). We see that, at variance with the other models, FOPT is here accurate even for rather large transition probabilities, of the order of 20%. We conclude that its application is much more reliable in the quasi-diabatic limit than in the quasi-adiabatic one.

	P_{12}		$\Delta\langle E\rangle$	
V_0	FOPT	num.	FOPT	num.
0.001	0.04744	0.04635	-0.001267	-0.001314
0.002	0.18976	0.17273	-0.001267	-0.001381
0.003	0.42697	0.34684	-0.001267	-0.001522

Table 3: Transition probabilities P_{12} and averaged energy differences $\Delta\langle E\rangle$ (a.u.) obtained for model II with different values of the interaction parameter V_0. All other parameters as in the example of Fig. 4. First-order perturbation theory (FOPT) predictions are compared with accurate numerical results.

5 Model III: photodissociation with an avoided crossing.

In this section we analyse a more realistic model, by solving it numerically. The aim is to throw a bridge between the quasi-adiabatic case (model I) and the quasi-diabatic one (model II). Moreover, we want to provide an example of what could be measured to confirm experimentally the energy selection effect.

The model describes the photodissociation of a diatomic molecule, so the coordinate q is the internuclear distance. We consider three adiabatic electronic states: the ground state $|0\rangle$ has a binding potential $U_0(q)$, while the two excited states $|1\rangle$ and $|2\rangle$ are dissociative and exhibit an avoided crossing. From the lowest vibrational state in U_0 we excite the molecule with a coherent light pulse to either state $|1\rangle$ or state $|2\rangle$. The ground state curve is a Morse function:

$$U_0(q) = E_{diss,0} \ \left[1 - e^{-\alpha(q-q_{eq})}\right]^2 \tag{53}$$

The excited adiabatic potential energy curves U_1 and U_2 are the eigenvalues of a 2x2 hamiltonian matrix expressed in a diabatic basis $|\eta_1\rangle, |\eta_2\rangle$. The matrix elements are:

$$\begin{aligned} H_{11}(q) &= \left\langle \eta_1 \middle| \hat{\mathcal{H}}_{el} \middle| \eta_1 \right\rangle = E_{diss,1} + A_1 \ e^{-\beta_1(q-q_{eq})} \\ H_{22}(q) &= \left\langle \eta_2 \middle| \hat{\mathcal{H}}_{el} \middle| \eta_2 \right\rangle = E_{diss,2} + A_2 \ e^{-\beta_2(q-q_{eq})} \\ H_{12}(q) &= \left\langle \eta_1 \middle| \hat{\mathcal{H}}_{el} \middle| \eta_2 \right\rangle = V_{12} \ e^{-\gamma(q-q_x)^2} \end{aligned} \tag{54}$$

with the parameters

$$\begin{array}{lll} E_{diss,0} = 2.0 \text{ eV} & \alpha = 0.6 \text{ a.u.} & q_{eq} = 4.0 \text{ bohr} \\ E_{diss,1} = 2.0 \text{ eV} & A_1 = 2.5 \text{ eV} & \beta_1 = 0.6 \text{ a.u.} \\ E_{diss,2} = 2.4 \text{ eV} & A_2 = 0.8 \text{ eV} & \beta_2 = 1.2 \text{ a.u.} \\ \gamma = 0.3 \text{ a.u.} & q_x = 6.91 \text{ bohr} & \end{array} \tag{55}$$

The maximum strength of the coupling, V_{12}, is varied in order to explore a range of conditions, from the quasi-diabatic one (small V_{12}) to the quasi-adiabatic (large V_{12}). As we can see in Fig. 5, the $H_{11}(q)$ and $H_{22}(q)$ curves cross at approximately q=6.91 bohr and the coupling $H_{12}(q)$ has its maximum at the same distance. Since the $H_{12}(q)$ gaussian function practically vanishes

at $q = q_{eq}$, in the Franck-Condon region the adiabatic and diabatic states practically coincide, namely $|1\rangle = |\eta_2\rangle$ and $|2\rangle = |\eta_1\rangle$. Moreover, the vertical excitation energies are not affected by the coupling strength V_{12}: $U_1(q_{eq}) - U_0(q_{eq}) = E_{diss,1} + A_1 = 4.5$ eV and $U_2(q_{eq}) - U_0(q_{eq}) = E_{diss,2} + A_2 = 3.2$ eV. The coupling also vanishes at large distances, so the dissociating wavepackets do not interact any more and their individual energies are well defined. At dissociation, $|1\rangle = |\eta_1\rangle$ and $|2\rangle = |\eta_2\rangle$.

We want to examine the dynamics following excitation to either $|1\rangle$ or $|2\rangle$, so in the first case we assume transition dipoles $\langle 0\,|\mu|\,1\rangle = 1$ a.u. (independent on q) and $\langle 0\,|\mu|\,2\rangle = 0$, and viceversa in the second case. The case in which both states carry oscillator strength shows very interesting interference effects[19,20] that would make the discussion of energy selection effects more complex. The light pulse is tuned to either the first or the second transition

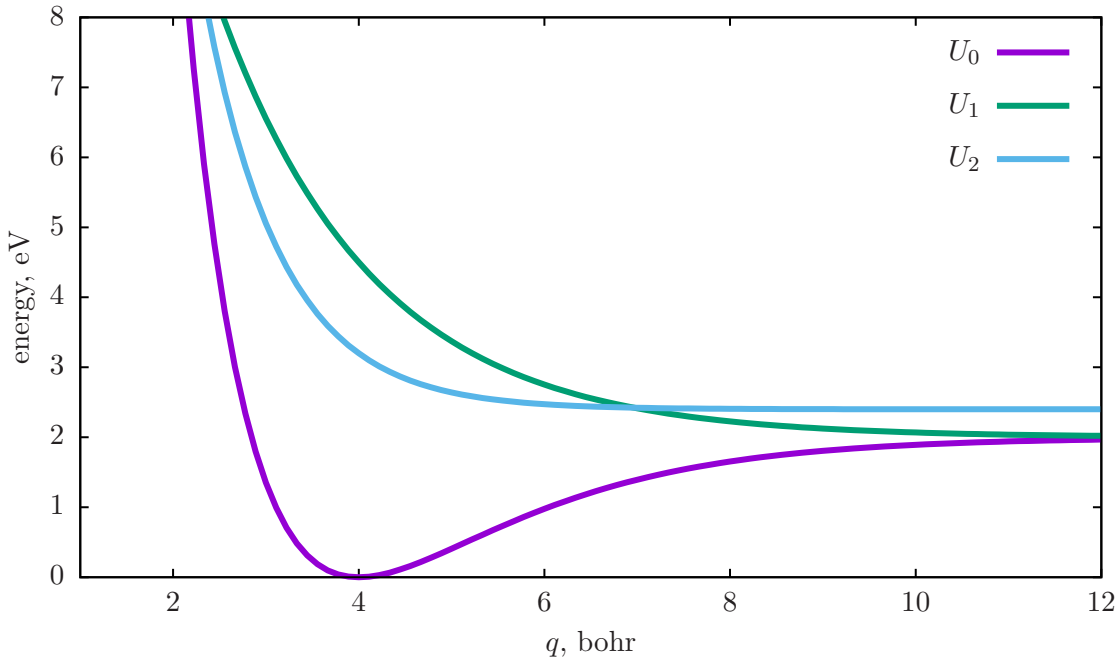

Figure 5: Adiabatic and diabatic potential energy curves for model III, with $V_{12} = 0.006$. The interaction H_{12} and the nonadiabatic coupling function g_{12} are shown in the inset.

energy and has a cosine envelope:

$$\begin{aligned} E(t) &= E_0 \, cos\left(\frac{\pi t}{2\tau}\right) \, cos(\Omega t) \qquad \text{for} \quad t \in [-\tau, \tau] \\ E(t) &= 0 \qquad\qquad\qquad\qquad\qquad\quad \text{for} \quad t \notin [-\tau, \tau] \end{aligned} \tag{56}$$

The duration of the pulse was chosen at $\tau = 2$ fs, because the associated frequency bandwidth is large enough as to produce a broad distribution of energies in the initial wavepacket, which is one of the basic requirements to observe the energy selection effect, as shown by eq. (23). We present below a few tests showing the effect of the pulse length.

The quantum wavepacket dynamic equations were solved in a numerically exact way by standard techniques.[15] We adopted the adiabatic representation and the coupling between the two excited adiabatic states was represented by the same operator as in section 3.2, eq. (26). In Fig. 5 we show the shape

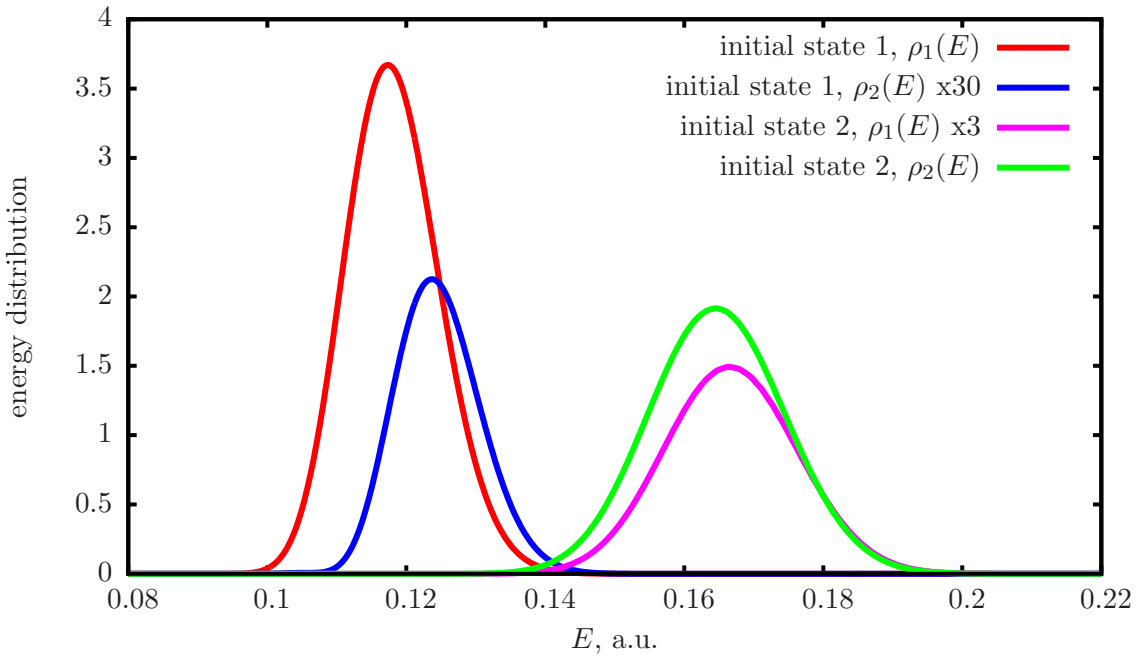

Figure 6: Energy distributions in the two adiabatic states obtained after the passage through the avoided crossing region with $V_{12} = 0.006$ a.u.

τ (fs)	initial state $\|1\rangle$	initial state $\|2\rangle$
1	0.0070	0.0025
2	0.0064	0.0020
5	0.0041	0.0008

Table 4: Energy differences $\Delta\langle E\rangle$ (a.u.) obtained for model III with $V_{12} = 0.006$ a.u. and three different pulse lengths τ.

of the g_{12} coupling function for $V_{12} = 0.006$. In all simulations, the reduced mass was 3000 a.u.

In Figure 6 we show the energy distributions obtained after the passage through the avoided crossing region with $V_{12} = 0.006$ a.u. We remind that these are total energies, made of the well defined electronic energy of the two dissociated atoms plus the kinetic energy of the nuclear wavepacket. We see an energy selection effect such that the distribution for the wavepacket that has undergone the nonadiabatic transition is displaced to higher energies. The effect is larger when we excite to the lower adiabatic state than to the higher one. This is consistent with two features we highlighted when analysing model I, namely (1) the energy selection is more effective for transitions from lower to upper state than viceversa, and (2) with a larger kinetic energy the required momentum change is smaller and therefore the process is less selective (see the discussion of eq. (23)). In the following we shall quantify the effect by computing averaged energy differences $\Delta\langle E\rangle$. They are taken as the expectation value of the molecular hamiltonian for the wavepacket that has undergone the nonadiabatic transition minus that of the wavepacket that has remained in the initial adiabatic state. In the example we have just discussed ($V_{12} = 0.006$ a.u.), we get $\Delta\langle E\rangle = 0.0064$ or 0.0020 a.u. when exciting to state $|1\rangle$ or to state $|2\rangle$, respectively.

We tested the effect of the pulse length by running calculations with $\tau =$ 1, 2 and 5 fs. Qualitatively the results remain the same, i.e. $\Delta\langle E\rangle$ is positive and is larger when we excite in state $|1\rangle$, but the energy selection effect decreases noticeably for the longest pulse duration because the spectrum of the exciting light becomes too narrow (see table 4). We only see a modest increase of $\Delta\langle E\rangle$ when decreasing τ below 2 fs, which indicates that the factor limiting the width of the energy spectrum of the excited wavepacket is the width of the absorption band. For this reason, in the following we shall

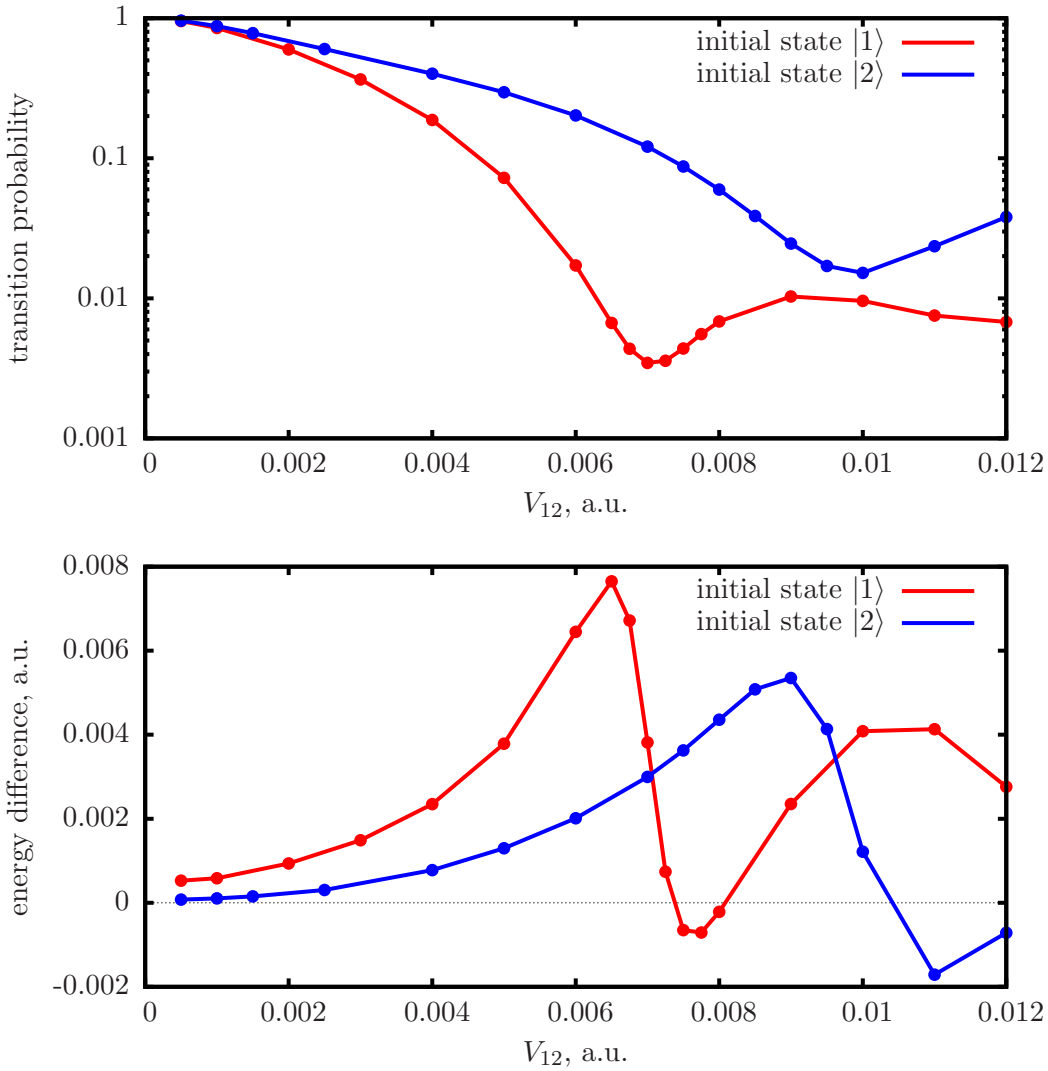

Figure 7: Transition probability P_f/P_i (upper panel) and average energy difference $\Delta\langle E\rangle$ between the final and the initial state (lower panel) as functions of V_{12} in model III. P_i is the population of the initial state just after the end of the radiation pulse ($t = 5$ fs), while P_f is the population of the other state after one passage through the avoided crossing region. The P_f and energy values are taken when $P_f(t)$ is well stabilized because the wavepacket has cleared the interaction region, which happens at $t = 60$ fs or at $t = 40$ fs if the initial state is $|1\rangle$ or $|2\rangle$, respectively.

present the results for $\tau = 2$ fs.

We further analysed the results as a function of V_{12}. Total transition probabilities between the adiabatic states and average energy differences are shown in Fig. 7. We find that for moderate values of V_{12}, $\Delta\langle E\rangle$ is positive, increasing with V_{12} and larger when the initial state is the lower one. At the same time, the transition probability decreases, showing a gradual evolution from the quasi-diabatic to the quasi-adiabatic regime. After reaching a maximum in $\Delta\langle E\rangle$, that roughly corresponds to a minimum in the transition probability, we observe a more irregular dependence on V_{12}. This is due to the fact that with large V_{12} the interaction region broadens to the point where the dynamics is far from what is expected for a typical avoided crossing.

In the region where $\Delta\langle E\rangle$ and the transition probability are monotonic functions of V_{12}, respectively increasing and decreasing, we can compare the numerical results of model III with the predictions for models Ib and II. To this aim, the parameters of models Ib and II are adapted to represent the avoided crossing discussed here, to begin with the reduced mass which is $m = 3000$ a.u. To obtain a wavepacket with the right kinetic energy when it goes through the avoided crossing region, we set

$$E_0 = E_{FC} - E_X \pm V_{12}$$

where: E_{FC} is the energy of the Franck-Condon point (0.1176 and 0.1649 a.u. respectively for states 1 and 2); $E_X = 0.0891$ a.u. is the energy of the crossing between the diabatic curves; the V_{12} term is negative for the higher state and positive for the lower one. We find that a width $\sigma_0 = 0.36$ bohr yields energy profiles in the initial state quite similar to those of model III. The D parameter of model Ib is taken equal in module to $2V_{12}$, i.e. approximately the minimum energy gap at the avoided crossing. The sign of D is positive when the initial state is 1 and negative when it is 2. The V_0 interaction of model II is simply identified with V_{12}. Finally, the parameters of the nonadiabatic coupling function g_{12}, eq. (25), are $W_0 = F/(2V_{12})$ where $F = 0.00859$ a.u. is the slope difference between the diabatic curves, and $\sigma_W = \sqrt{\pi}V_{12}/(2F)$. This corresponds to a typical avoided crossing where the area under the $g_{12}(q)$ curve is $\pi/2$.

For small values of V_{12}, i.e. when the dynamics is nearly diabatic, the term of comparison is model II. With the parameters adopted here, model II yields $\Delta\langle E\rangle \simeq 0.00065$ a.u. and this result is nearly independent on V_{12} and

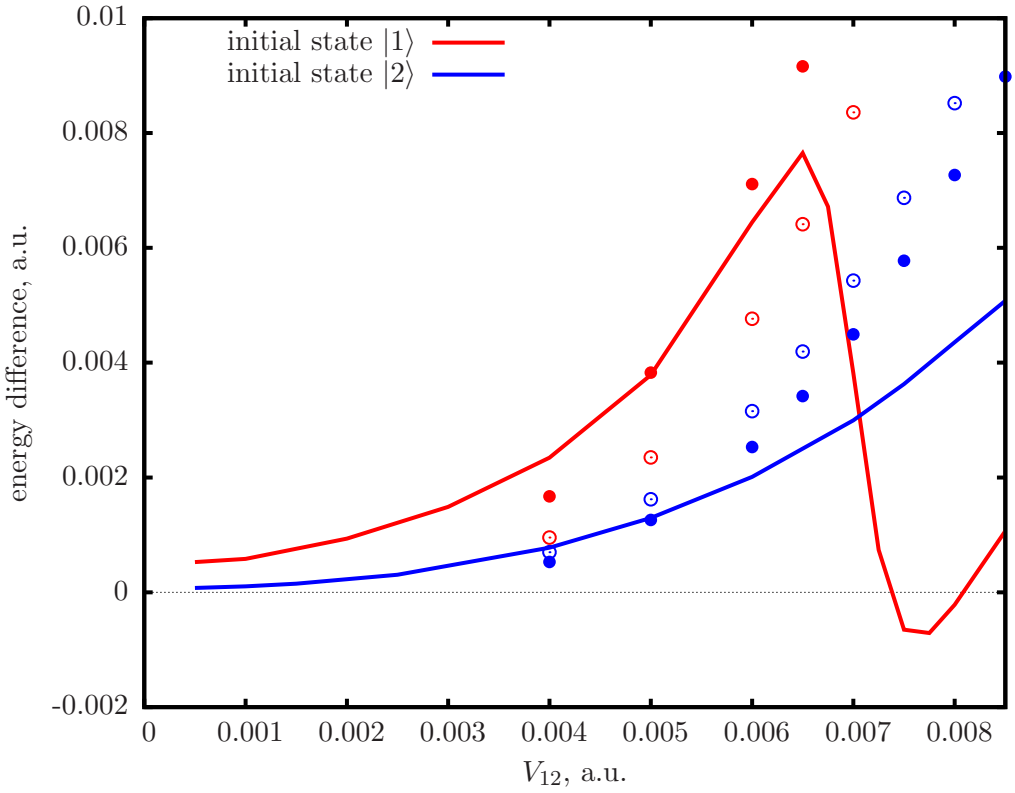

Figure 8: Average energy difference $\Delta\langle E\rangle$ between the final and the initial state as a function of V_{12} in model III. Red and blue full dots show the results of model Ib, obtained respectively for excitation to the lower and upper states. Red and blue open circles show results obtained in the same way, except that the kinetic energy of the wavepacket is set to the same value irrespective of the starting state.

on the choice of the initial state, for the reasons discussed in section 4. Note that here the initial state also affects E_0, but $\Delta\langle E\rangle$ has been shown not to depend on this parameter within model II. Therefore, although the predicted value of $\Delta\langle E\rangle$ is of the right order of magnitude, this model cannot account for the difference between the $1 \to 2$ and $2 \to 1$ nonadiabatic processes.

More interesting is the comparison with model Ib, for which the perturbative solution is valid with larger values of D. As already stated, here $|D|$ is assimilated with $2V_{12}$. Some values of $\Delta\langle E\rangle$, computed by means of eqs. (13) and (30), are shown by red and blue dots in Fig. 8. Although the de-

pendence of $\Delta\langle E\rangle$ on V_{12} appears to be overestimated (the same is true for the transition probabilities, that decrease too fast), the trend is fairly well reproduced. Two factors concur in yielding a larger $\Delta\langle E\rangle$ when the molecule is excited to the lower state: one is the fact that the upward nonadiabatic transitions show a more effective energy selection than the downward ones; the other is the larger kinetic energy available when exciting to the upper state, which decreases the energy/momentum matching effect (see section 3). In order to estimate the relative importance of these two factors, we computed again $\Delta\langle E\rangle$ according to model Ib, but using the same $E_0 = 0.0522$ a.u. (an average value) for both initial states. The results are shown by red and blue open circles in Fig. 8. The difference in $\Delta\langle E\rangle$ between exciting to the lower versus the upper state is still noticeable, but is reduced to 20%-50% of the previous values. We can conclude that both factors are important, but in this example the difference in the kinetic energies is more effective than the upward versus downward direction of the transition.

6 Surface hopping and energy selection.

We ran surface hopping (SH) simulations on model III, in order to show how the energy selection effect is reproduced by this popular method of semiclassical dynamics. Our version of SH includes "overlap-based" decoherence corrections (ODC) that usually improve the agreement with fully quantum mechanical (QM) nonadiabatic transition probabilities.[12] We found that in the case of model III the parameter σ, i.e. the width of the virtual wavepackets that the ODC algorithm associates with classical points in the nuclear phase space, must be quite small (we chose $\sigma = 0.02$ bohr). Such a small σ implies a very short decoherence time, which seems to be consistent with two features of the model: a very fast transit of the wavepacket through the strong interaction region; and, the alternation of negative and positive signs of the $g_{12}(q)$ function, that in the absence of decoherence leads to an underestimation of the transition probability. The excitation with the ultrashort light pulse was simulated by vertical transitions from a Wigner distribution of phase space points in the ground state.[13]

We ran SH simulations (each one made of 10^4 trajectories) for some representative values of V_{12}. The nonadiabatic transition probabilities P_{IJ} and the $\Delta\langle E\rangle$ values obtained by averaging over the trajectories belonging to each electronic state are shown in Table 5. For comparison, we also list the

Initial excitation to state 1				
V_{12}	P_{12}		$\Delta\langle E\rangle$	
	SH	QM	SH	QM
0.002	0.515	0.598	0.00155	0.00094
0.003	0.325	0.366	0.00130	0.00149
0.004	0.230	0.188	0.00132	0.00235
Initial excitation to state 2				
V_{12}	P_{21}		$\Delta\langle E\rangle$	
	SH	QM	SH	QM
0.002	0.714	0.688	0.00164	0.00022
0.003	0.479	0.527	0.00172	0.00043
0.004	0.332	0.401	0.00160	0.00078

Table 5: Nonadiabatic transition probabilities P_{IJ} and averaged energy differences $\Delta\langle E\rangle$ (a.u.) between the final and the initial state, as functions of V_{12} (a.u.).

corresponding QM results. It is clear that the $\Delta\langle E\rangle$ values computed by SH, although of the right order of magnitude and sign, do not increase with V_{12} as the QM ones. Also the larger energy selection effect characterizing upward versus downward transitions is not reproduced, on the contrary SH yields slightly smaller $\Delta\langle E\rangle$ for the upward transition. These two failures are due to the fact that in surface hopping, as in Landau-Zener theory, the transition probability does not take into account the momentum/energy matching factor. Although a larger energy gap tends to decrease the transition probability, there is no difference between upward and downward hops. While the transition probability in SH depends on the nuclear momentum through its scalar product with the nonadiabatic coupling vector, the kinetic energy as such is not considered. Only after a hop has taken place, the kinetic energy is usually readjusted to guarantee energy conservation, as we did in this work, but this operation does not affect the hopping probability, nor does it introduce a difference between upward and downward hops (except in the case of "frustrated hops"[10,11] that are anyway rare when decoherence corrections are applied[12]).

These findings suggest that the surface hopping algorithms may be improved by taking into account the energy/momentum matching in the determination of the hopping probability. For instance, large momentum changes might be forbidden or made less probable. The goal would be not only to im-

prove the treatment of energy selection, but rather to make surface hopping more consistent with the physical reality.

7 Conclusions.

In this work we show that nonadiabatic transitions between two electronic states are possibly associated with energy selection effects. By this we mean that the component of the time-dependent wavefunction undergoing the transition has an energy distribution markedly different from the other one. We investigate this issue by three one-dimensional models. Two are very schematic models that can represent the quasi-adiabatic and quasi-diabatic behaviours, respectively, and are analysed with the help of first-order perturbation theory. The third is a more realistic model for the photodissociation of a diatomic molecule in states undergoing an avoided crossing, such that all regimes from quasi-diabatic to quasi-adiabatic can be spanned. This model is treated numerically.

The predictions of the two solvable models and the numerical results of the third one provide a consistent picture of the energy selection effect. The average total energy of the wavepacket that undergoes the transition tends to be higher than that of the wavepacket that remains in the initial state, even if the electronic energy has decreased (downward transition). The energy difference between the two final wavepackets is however larger for upward transitions and it increases with the energy gap between the two electronic states. As a result, large energy differences are associated with small transition probabilities between adiabatic states.

Probably the most appropriate way to detect this effect experimentally is to perform the photodissociation of a diatomic molecule that could yield atomic fragments in two different final states. The measurement of their kinetic energy by a state selective spectroscopy, for instance LIF with sub-Doppler resolution, should provide the total energy (i.e. electronic plus nuclear kinetic energy) for the two channels. Ideally, the molecular electronic states should exhibit an avoided crossing that splits the dissociating wavepacket in the two channels. To obtain a fairly large energy difference one should accept a small yield (say $< 10\%$) in the channel that is populated by the nonadiabatic transition. Since the effect is based on the selection of different energy components in a nuclear wavepacket, the latter should have a sufficiently broad energy spectrum, hence the need for ultrashort pump

pulses, of the order of few femtoseconds.

Acknowledgments

This research was supported by funds of the University of Pisa.

References

[1] Ranitovic, P.; Hogle, C. W.; Rivière, P.; Palacios, A.; Tong, X.-M.; Toshima, N.; González-Castrillo, A.; Martin, L.; Martín, F.; Murnane, M. M.; Kapteyna, H. Attosecond vacuum UV coherent control of molecular dynamics. *Proc. Natl. Acad. Sci.* **2014**, *111*, 912.

[2] Elsaesser, T. Ultrafast processes in chemistry. *Chem. Rev.* **2017**, *117*, 10621.

[3] Nakamura, H. *Nonadiabatic Transition: Concepts, Basic Theories and Applications*, World Scientific, 2012

[4] Bourquin, R.; Gradinaru, V.; Hagedorn, G. A. Non-adiabatic transitions near avoided crossings: theory and numerics. *J. Math. Chem.* **2012**, *50*, 602.

[5] Ferretti, A.; Granucci, G.; Lami, A.; Persico, M.; Villani, G. Quantum mechanical and semiclassical dynamics at a conical intersection. *J. Chem. Phys.* **1996**, *104*, 5517.

[6] Cattaneo, P.; Persico, M. Wave packet dynamics in the presence of a conical intersection. *J. Phys. Chem. A* **1997**, *101*, 3454.

[7] Makhov, D. V.; Saita, K.; Martinez, T. J.; Shalashilin, D. V. Ab initio multiple cloning simulations of pyrrole photodissociation: TKER spectra and velocity map imaging. *Phys. Chem. Chem. Phys.* **2015**, *17*, 3316.

[8] Grebenshchikov, S. Yu.; Picconi, D. Fano resonances in the photoinduced H-atom elimination dynamics in the $\pi\sigma^*$ states of pyrrole. *Phys. Chem. Chem. Phys.* **2017**, *19*, 14902.

[9] Park, K.; Engelkemier, J.; Persico, M.; Manikandan, P.; Hase, W. L. Algorithms for Sampling a Quantum Microcanonical Ensemble of Harmonic Oscillators at Potential Minima and Conical Intersections. *J. Phys. Chem. A* **2011**, *115*, 6603-6609.

[10] Fang, J.-Y.; Hammes-Schiffer, S. Improvement of the internal consistency in trajectory surface hopping. *J. Phys. Chem. A* **1999**, *103*, 9399.

[11] Parandekar, P. V.; Tully, J. C. Mixed quantum-classical equilibrium. *J. Chem. Phys.* **2005**, *122*, 094102.

[12] Granucci, G.; Persico, M.; Zoccante, A. Including quantum decoherence in surface hopping. *J. Chem. Phys.* **2010**, *133*, 134111/1-9.

[13] Granucci, G.; Persico, M. An overview of nonadiabatic dynamics simulations methods, with focus on the direct approach versus the fitting of potential energy surfaces. *Theoret. Chem. Acc.* **2014**, *133*, 1526.

[14] Tannor, D. J. *Introduction to Quantum Mechanics: a Time-Dependent Perspective*, University Science Books, 2007

[15] Magnier, S.; Persico, M.; Rahman, N. Theoretical study of two-photon above threshold dissociation and related processes in Na_2^+ and Li_2^+. *J. Phys. Chem. A* **1999**, *103*, 10691.

[16] The function $\frac{\partial g_{ij}}{\partial q}$ in eq. 26 replaces the matrix element $\left\langle \psi_i \left| \frac{\partial^2}{\partial q^2} \right| \psi_j \right\rangle$ of the general formula in the special case of two states.[17] In fact, for more electronic states we have: $\left\langle \psi_i \left| \frac{\partial^2}{\partial q^2} \right| \psi_j \right\rangle = \sum_{k \neq i,j} g_{ik} g_{kj} + \frac{\partial g_{ij}}{\partial q}$. Of these two terms, the first one is hermitian and the latter is needed to guarantee the hermiticity of the whole operator (26). In a two-state model where the couplings with other electronic states are neglected, the diagonal matrix elements simplify to $\left\langle \psi_i \left| \frac{\partial^2}{\partial q^2} \right| \psi_i \right\rangle = \left\langle \psi_j \left| \frac{\partial^2}{\partial q^2} \right| \psi_j \right\rangle = -g_{ij}^2$ and the off diagonal ones to $\left\langle \psi_i \left| \frac{\partial^2}{\partial q^2} \right| \psi_j \right\rangle = -\left\langle \psi_j \left| \frac{\partial^2}{\partial q^2} \right| \psi_i \right\rangle = \frac{\partial g_{ij}}{\partial q}$.

[17] de Vivie-Riedle, R.; Hofmann, A. Nonadiabatic quantum dynamics and control strategies. *Adv. Ser. Chem. Phys.* **2004**, *15*, 803.

[18] Vallée, O.; Soares, M. *Airy functions and applications to physics*, Imperial College Press, 2004.

[19] Granucci, G.; Persico, M. Coherent excitation of wavepackets in two electronic states. Interference effects at an avoided crossing. *Chem. Phys. Lett.* **1995**, *246*, 228.

[20] Romstad, D.; Granucci, G.; Persico, M. Nonadiabatic transitions and interference in photodissociation dynamics. *Chem. Phys.* **1997**, *219*, 21.

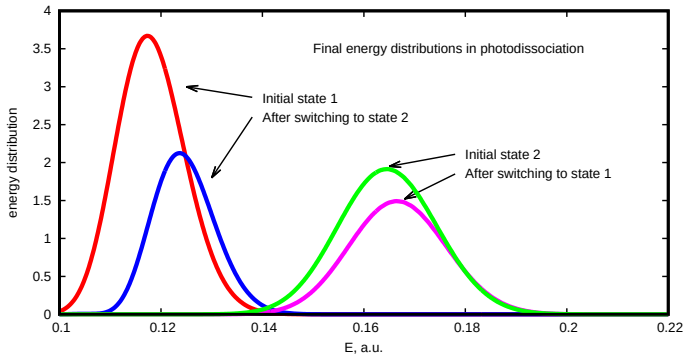
Final energy distributions in photodissociation
Initial state 1
After switching to state 2
Initial state 2
After switching to state 1
energy distribution
E, a.u.
0
0.5
1
1.5
2
2.5
3
3.5
4
0.1
0.12
0.14
0.16
0.18
0.2
0.22

Energy selection in nonadiabatic transitions.

G. Granucci, G. Melani, M. Persico, P. Van Leuven

Supporting Information.

Comparison between models Ib, II and III.

The numerical results of model III are here compared with those of models Ib and II, based on perturbation theory. To this aim, the parameters of the two models Ib and II are adapted to represent the avoided crossing of section 5. The reduced mass is in all cases $m = 3000$ a.u. To obtain a wavepacket with the right kinetic energy when it goes through the avoided crossing region, we set

$$E_0 = E_{FC} - E_X \pm V_{12}$$

where:

- E_{FC} is the energy of the Franck-Condon point (0.1176 and 0.1649 a.u. respectively for states 1 and 2);
- $E_X = 0.0891$ a.u. is the energy of the crossing between the diabatic curves;
- the V_{12} term is negative for the higher state and positive for the lower one.

We find that a width $\sigma_0 = 0.36$ bohr yields energy profiles in the initial state quite similar to those of model III. The D parameter of model Ib is taken equal in module to $2V_{12}$, i.e. approximately the minimum energy gap at the avoided crossing. The sign of D is positive when the initial state is 1 and negative when it is 2. The V_0 interaction of model II is simply identified with V_{12}. Finally, the parameters of the nonadiabatic coupling function g_{12}, eq. (25), are $W_0 = F/(2V_{12}$ where $F = 0.00859$ a.u. is the slope difference between the diabatic curves, and $\sigma_W = \sqrt{\pi}V_{12}/(2F)$. This corresponds to a typical avoided crossing where the area under the $g_{12}(q)$ curve is $\pi/2$.

For small values of V_{12}, i.e. when the dynamics is nearly diabatic, the term of comparison is model II. With the parameters adopted here, model II yields $\Delta\langle E\rangle \simeq 0.00065$ a.u. and this result is nearly independent on V_{12} and on the choice of the initial state, for the reasons discussed in section 4. Note that here the initial state also affects E_0, but $\Delta\langle E\rangle$ has been shown not to depend on this parameter within model II. Therefore, although the predicted

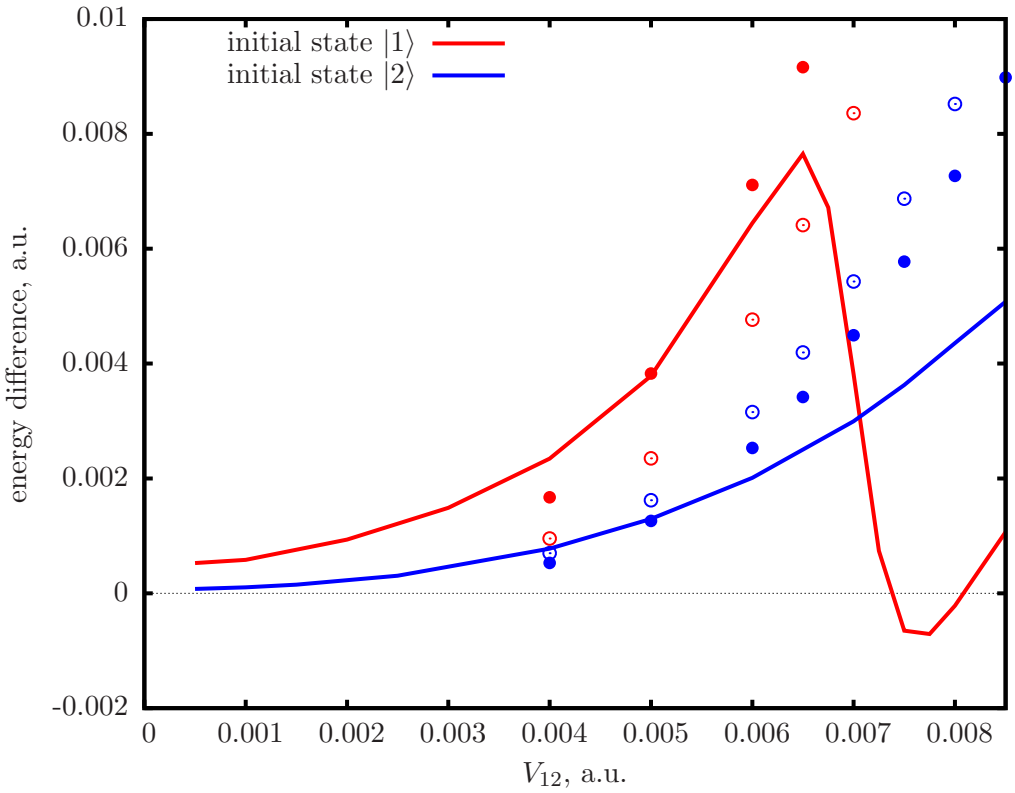

Figure S1: Average energy difference $\Delta\langle E\rangle$ between the final and the initial state as a function of V_{12} in model III. Red and blue full dots show the results of model Ib, obtained respectively for excitation to the lower and upper states. Red and blue open circles show results obtained in the same way, except that the kinetic energy of the wavepacket is set to the same value irrespective of the starting state.

value of $\Delta\langle E\rangle$ is of the right order of magnitude, this model cannot account for the difference between the $1 \to 2$ and $2 \to 1$ nonadiabatic processes.

More interesting is the comparison with model Ib, for which the perturbative solution is valid with larger values of V_{12}. Some values of $\Delta\langle E\rangle$, computed by means of eqs. (13) and (28), are shown by red and blue dots in Fig. S1. Although the dependence of $\Delta\langle E\rangle$ on V_{12} appears to be overestimated (the same is true for the transition probabilities, that decrease too fast), the trend is fairly well reproduced. Two factors concur in yielding a larger $\Delta\langle E\rangle$ when the molecule is excited to the lower state: one is the fact that the upward nonadiabatic transitions show a more effective energy selection than the downward ones; the other is the larger kinetic energy available when exciting to the upper state, which decreases the energy/momentum matching effect (see section 3). In order to estimate the relative importance of these two factors, we computed again $\Delta\langle E\rangle$ according to model Ib, but using the same $E_0 = 0.0522$ a.u. (an average value) for both initial states. The results are shown by red and blue open circles in Fig. S1. The difference in $\Delta\langle E\rangle$ between exciting to the lower versus the upper state is still noticeable, but is reduced to 20%-50% of the previous values. We can conclude that both factors are important, but in this example the difference in the kinetic energies is more effective than the upward versus downward direction of the transition.